



Computations of flow and heat transfer in a three-dimensional multilouvered fin geometry

J. Cui ^a, D.K. Tafti ^{b,*}

^a Department of Mechanical Engineering, Center for Electric Power, Tennessee Technological University, Cookeville, TN 38505, USA

^b Department of Mechanical Engineering, Virginia Tech, 105 Randolph Hall, Blacksburg, VA 24061, USA

Received 10 August 2001; received in revised form 16 May 2002

Abstract

This study presents computational results in a complex three-dimensional louver geometry. The three-dimensionality occurs along the height of the fin, where the angled louver transitions to the flat landing and joins with the tube surface. The transition region is characterized by a swept leading edge and decreasing flow area between louvers. The results show that for $Re_b = 1100$, the flow on the angled louver is dominated by spanwise vortex shedding, which is weakly three-dimensional. On the other hand, the flow in the transition region exhibits strong three-dimensionality. A high-energy compact vortex jet forms in the vicinity of the louver junction with the flat landing and is drawn under the louver. The top surface experiences large velocities in the vicinity of the surface and exhibits high heat transfer coefficients. Although the flow slows down at the flat landing, the large induced velocities on the top surface increases the heat transfer coefficient on the tube surface.

© 2002 Elsevier Science Ltd. All rights reserved.

1. Introduction

Multilouvered fins are used extensively in the automobile and heating, ventilation and air-conditioning (HVAC) industries for enhancing air-side heat transfer in compact heat exchangers. They can be manufactured by high-speed production techniques and are more economical than other interrupted fin geometries. Researchers from universities and from the HVAC and automotive industries have published considerable amount of experimental visualizations and measurements, empirical correlations, and numerical simulations in this area. A review of past experimental and computational work can be found in Tafti et al. [1,2].

The heat transfer in multilouvered fins is influenced by three factors: (a) duct versus louver directed flow [3,4]; (b) thermal wake interference [5]; (c) flow instabilities and transport of coherent vorticity in the vicinity of the louver surface [6]. These three phenomena can be captured with good precision in two-dimensional unsteady simulations. Factors (a) and (b) are primarily dependent on the two-dimensional geometrical parameters. The onset of unsteadiness is primarily a two-dimensional phenomenon, which can either be classified as a wake or Kelvin–Helmholtz instability [7], and can be resolved with accuracy in the initial stages of development. However, there is evidence [8–10], that as the Reynolds number increases beyond Re_{D_h} (based on hydraulic diameter) of about 2000–2500, secondary three-dimensional instabilities may be important. The intrinsic three-dimensionality, which develops in the flow field, cannot be resolved with two-dimensional simulations. It has the effect of reducing the coherence of the vortical structures, hence reducing their effectiveness in enhancing heat transfer.

Other than the intrinsic three-dimensionality that could develop at high Reynolds numbers, additional three-dimensionality is inherent in the multilouvered geometry near the junction of the louver with the tube

* Corresponding author. Tel.: +1-540-231-9975; fax: +1-540-231-9100.

E-mail address: dtafti@vt.edu (D.K. Tafti).

Nomenclature

b	non-dimensional fin thickness (b^*/L_p^*)	t	non-dimensional time, $t = t^*u_\tau^*/L_p^*$
f	non-dimensional characteristic frequency ($f^*L_p^*/u_\tau^*$)	u_τ^*	friction velocity
F_p^*	dimensional fin pitch	u_b^*	bulk velocity
F_p^*	non-dimensional fin pitch (F_p^*/L_p^*)	V_c^*	maximum bulk velocity based on nominal flow area in louver bank
j	Colburn factor $j = Nu/Re_b Pr^{0.4}$	x, y, z	non-dimensional coordinates, $x = x^*/L_p^*$, $y = y^*/L_p^*$, $z = z^*/L_p^*$
L_p^*	dimensional louver pitch (characteristic length scale)	<i>Greek symbols</i>	
Nu	Nusselt number, $Nu = (L_p^*q''/(T_s^* - T_{ref}^*))/\kappa$	α	thermal diffusivity
Pr	Prandtl number	κ	thermal conductivity
q''	heat flux	ν	kinematic viscosity
Re_τ	Reynolds number ($u_\tau^*L_p^*/\nu$)	θ	fluctuating non-dimensional temperature about the mean
Re_b	Reynolds number ($u_b^*L_p^*/\nu$)	<i>Superscript</i>	
Re_{L_p}	Reynolds number ($V_c^*L_p^*/\nu$)	*	dimensional quantities
T_s^*	surface temperature		
T_{ref}^*	reference temperature, integrated mixed mean		
T	non-dimensional temperature, $T = T^*/(q''L_p^*/\kappa)$		

surface, along the height of the fin in flat tube heat exchangers. The angled louver transitions to a flat landing, which extends to the tube surface as shown in Fig. 1.¹ The extent of the transition region is estimated to be $0.5L_p^*$ [11]. A consequence of the manufacturing process is that the leading and trailing edges of the louver in the transition region, instead of being normal to the flow direction, exhibit a “sweep” angle to the flow direction. In addition to this effect, the open flow area between two subsequent louvers is restricted as the louvers approach the flat landing.

The objective of the present study is to perform high-resolution time-dependent simulations in the three-dimensional louver geometry by explicitly taking into account the transition region from louver to the tube surface, and to identify to what extent this junction affects the flow field and heat transfer, both locally and globally. In corrugated fins, the flow in this region is also important from the point of view of condensate management and carryover [12].

The paper is organized as follows: in the next section, a brief description of the numerical and computational method is given, followed by validation of the computational results. The results are presented by first introducing the unsteady dynamics of flow and heat transfer, followed by the mean time-averaged effects.

2. Numerical formulation and computational details

The governing flow and energy equations are non-dimensionalized by a characteristic length scale, which in this case is taken to be the louver pitch, L_p^* , the friction velocity, $u_\tau^* = \sqrt{\Delta p_x^*/\rho}$ as the velocity scale, and $q''L_p^*/\kappa$ as the temperature scale. Here, Δp_x^* is the mean pressure gradient in the streamwise direction, q'' is the specified dimensional constant heat flux on the louver and tube surface, and κ is the thermal conductivity of the fluid. The above non-dimensionalization results in a Reynolds number based on the friction velocity $Re_\tau = u_\tau^*L_p^*/\nu$, and Prandtl number $Pr = \nu/\alpha$, where ν and α are the kinematic viscosity and thermal diffusivity of the fluid, respectively.

For computational purposes, fully developed flow and thermal conditions are assumed in the multilouvered fins. The louvered fin geometry is approximated by an infinite array of louvers in both streamwise and cross-stream directions, which results in a simpler system with periodic repetition of the basic unit. The fully developed flow and heat transfer regime is experimentally observed to be attained by the second row in the streamwise direction for parallel-plate fins [13], and by the third or fourth row for louvered fins [14]. The unit computational domain for the base louver geometry has a dimension of 1 (normalized by louver pitch L_p^*) in streamwise (x) direction, fin pitch 1 (in this particular case, fin pitch F_p^* is same as L_p^*) in cross-stream (y) direction, and 2.5 in spanwise (z) direction, as shown in Fig. 1(a). Along the spanwise direction, the louver can be divided into three parts: angled louver (length is 1.75),

¹ In corrugated fins, the “flat landing” is not flat but curves at the junction with the tube. For current purposes we assume that the landing is flat.

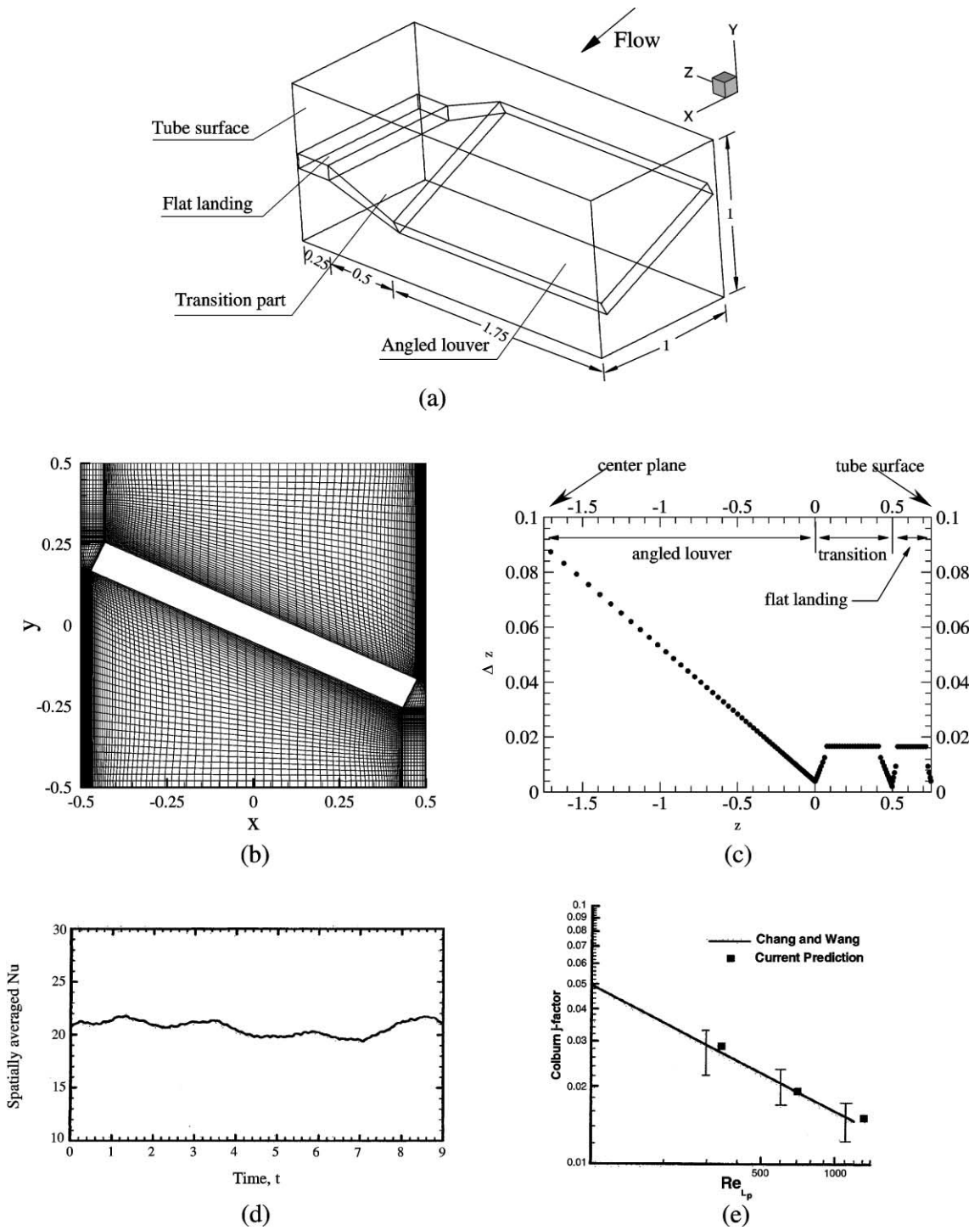


Fig. 1. (a) Computational domain consisting of one louver representing an infinite array of louvers put together in the streamwise and cross-stream directions; (b) computational mesh in a z -plane; (c) grid distribution in the spanwise direction along the fin height, more grid points are distributed at the junction between the angled louver and transition region, and between transition region and flat landing; (d) temporal evolution of the spatially averaged Nusselt number. The flow has adjusted to the mean pressure gradient and reached a statistically stationary state; (e) comparison of calculated j -factors with CW correlation. $Re_{L_p} = 1200$ corresponds to the calculation reported in this paper.

transition part (length is 0.5), and flat landing (length is 0.25). A linear transition profile is prescribed between the angled louver and the flat landing [15]. The thickness of the louver is 0.1 with 25° louver angle.

Periodic boundary conditions for velocity, modified pressure and temperature are applied in the streamwise and cross-stream directions since the flow is assumed to be both hydrodynamically and thermally fully developed without any entrance or exit effects. The application of periodic boundary conditions in the streamwise direction requires that pressure and temperature be reformulated as in Patankar et al. [16]. No-slip, no-penetration boundary conditions for velocity and constant heat flux conditions are enforced on the louver surface and the tube surface. Along the fin height at a distance of 2.5 from the tube wall, it is assumed that the flow is sufficiently removed from the extrinsic three-dimensional effects of the transition region and is nominally two-dimensional. This facilitates the application of symmetry boundary conditions. Our results show that this assumption is well justified.

The governing equations for momentum and energy are discretized with a conservative finite volume formulation using a second-order central difference scheme. A non-staggered grid topology is adopted. The Cartesian velocities, pressure, and temperature are calculated and stored at the cell center, whereas contravariant fluxes are stored and calculated at the cell faces. For the time integration of the discretized continuity and momentum equations, a projection method is used [17]. The temporal advancement is performed in two steps, a predictor step, which calculates an intermediate velocity field, and a corrector step, which calculates the updated velocity at the new time step by satisfying discrete continuity. The energy equation is advanced in time by the predictor step.

The computational mesh consists of 98 zones in ξ - and η -directions, respectively, and 128 zones in ζ -direction along the fin height. The grid is clustered in the vicinity of the louver, in the transition zone and tube wall region for better resolution. The mesh is partitioned into 16 blocks in the spanwise direction. Each block ($98 \times 98 \times 8$) is assigned to a processor in a distributed programming environment. The calculations are performed on 16 processors of SGI-Cray Origin 2000. The Reynolds number, Re_τ , is 400, which gives a bulk Reynolds number Re_b , based on the calculated bulk velocity and louver pitch, of approximately 1100. This lies at the high end in typical applications. The time step used in the computation is 5×10^{-5} . Initial conditions are obtained from an analogous two-dimensional simulation over the angled louver. The two-dimensional solution is replicated in the spanwise direction along the height of the fin. Since the flow rate adjusts to the imposed pressure gradient, it is much more economical to run a

separate two-dimensional simulation, which gives a fairly good estimate of the bulk flow velocity to begin with, than to simulate the same transient process in the three-dimensional calculations.

The flow at this Reynolds number is also time-dependent. Hence the flow not only has to adjust to the mean pressure gradient but also reach a statistically stationary state. Time series data of field variables are carefully monitored and stationarity is claimed when these data show a near constant mean value or a quasi-periodic fluctuation in time. Fig. 1(d) shows the stationary time evolution of the spatially averaged Nusselt number calculated on the louver surface for the last 9 time units of the simulation. Stationarity is well established with a mean value around 20 with a maximum fluctuation within 5% of the mean value. Unless otherwise noted, all mean quantities are obtained by averaging over the last three non-dimensional time units (from time $t = 6-9$).

To characterize the heat transfer, we define a local instantaneous Nusselt number. The surface-averaged Nusselt number is obtained by integration over the louver surface. In this paper, reference to the surface-averaged Nusselt number refers to the entire louver surface (excluding tube surface), whereas locally surface-averaged Nusselt number refers to the average Nusselt number in each computational block.

More details of the numerical algorithm, treatment of the boundary conditions, verification of the computer program and domain decomposition for parallel computing can be found in Tafti et al. [1,2].

3. Validation of numerical results

Numerical accuracy and resolution are crucial issues in time-dependent calculations in complex geometries. More often than not, quantitative validation of the calculation is challenging because of the lack of detailed three-dimensional experimental data, the expense and inability to perform grid independency studies, and by the lack of a-priori knowledge of the flow field. The three-dimensional louver geometry has the potential for generating highly complex and three-dimensional flow and thermal fields. Hence, a-priori, the grid must be designed intelligently such that energetic eddies are appropriately resolved. To do this we have drawn on our experience with two-dimensional unsteady simulations [6], where we have established through grid refinement studies, that a mesh resolution of 96×96 computational cells in the z -plane surrounding a louver is sufficiently fine to capture all the important dynamics of flow oscillations. Fig. 1(b) shows the computational mesh in a z -plane in the angled louver portion. The grid is clustered in the vicinity of the louver with the first grid point above the louver surface at 0.0019 (in non-dimensional

unit), which falls between 0.1 and 0.3 in local wall units² based on the local shear stress. In the region with the highest shear stress (in the transition region), there are five grid points within 10 wall units normal to the surface, with the first one at 0.3. Attention has also been given to the grid distribution in the streamwise and spanwise directions. Along the streamwise direction, the grid is nearly uniform with spacing of 5–7 wall units. Along the fin height or spanwise direction, the mesh distribution is clustered in the transition region and the tube surface. Fig. 1(c) shows the spanwise grid distribution Δz versus z . The mesh is coarsest in the two-dimensional region of the geometry with the maximum spacing of 60 wall units and finest at the beginning and end of transition, and near the tube wall with the spacing around 3 wall units. This gives us confidence that the boundary layers on the louver and tube surface are very well resolved. Since most of the energy is adequately resolved, there is no need to use any subgrid-scale stress models.

Another validation is to check the force balance on the louver. In the current simulation, a mean pressure gradient is imposed in the streamwise direction to drive the flow. Consequently, this pressure force should be balanced by the sum of the form (pressure) drag force and friction drag force from the louver surface and the friction drag force from the tube surface. The form drag acting on the louver surface is nearly three times the friction drag, which is fairly typical of louver geometries. The force balance between the imposed force and the forces from the louver and tube surface is verified (with an error at 0.6%). This validates the numerical formulation and the adequacy of the time averaging sample size.

Finally we compare the calculated overall Colburn j -factor (louver + tube) with the correlation of Chang and Wang [18] (CW). This is a general correlation developed from experimental data available for different types of louver geometries. The following geometrical values are used in the correlation (all lengths are normalized by louver pitch): $F_p = 1$, $\theta = 25^\circ$, $b = 0.1$, fin height = tube pitch = 5, tube depth = 15, and louver length = 4.5.³ Fig. 1(e) plots the j -factor for three calculated Reynolds numbers, from which the largest corresponds to the calculation reported in this paper. Also plotted

are upper and lower bounds of the experimental data from which the CW correlation was derived. The calculated j -factors are well within experimental scatter, and in fact compare quite well with the correlation.

4. Results

The imposed pressure gradient of unity and $Re_\tau = 400$, give a calculated bulk Reynolds number Re_b of approximately 1100. In general the flow is unsteady with self-sustained flow oscillations. The flow oscillations manifest themselves as spanwise vortices, which are nominally two-dimensional in nature with weak three-dimensionality across the fin height. In the transition region, the flow exhibits strong three-dimensionality with additional unsteady phenomena. For the most part, the flow encountered at this Reynolds number, lie in the unsteady laminar to chaotic regimes.

First, the unsteady phenomenon governing flow and heat transfer are discussed and then their effect on the mean flow and thermal fields is presented.

4.1. Coherent vorticity dynamics

To characterize the unsteady nature of the flow and the associated vorticity dynamics, the $\nabla \mathbf{u}$ [19] vortex identification technique is used. The method has been used by a number of researchers in extracting coherent vorticity [10,20]. This frame-invariant method identifies vortical structures as regions of large vorticity, where rotation dominates over strain to cause the rate-of-deformation tensor $\nabla \mathbf{u}$ (velocity gradient tensor) to have complex eigenvalues (one real and two conjugate complex eigenvalues). The complex eigenvalues imply that the local streamline pattern is closed or spiral, thus correctly eliminating near-wall shear layers. This methodology can also be separately applied in the x -, y -, or z -planes in order to identify streamwise, cross-flow, and spanwise vortices [10], respectively. The strength of the vortex is measured in terms of the imaginary part of the eigenvalue of the velocity gradient tensor and is denoted by λ_i . The strength of its three subsets, streamwise, cross-flow, and spanwise vortices is measured in terms of the imaginary part of the eigenvalue of the velocity gradient on the x -, y -, and z -planes, respectively, and is denoted by $\lambda_{i,x}$, $\lambda_{i,y}$, and $\lambda_{i,z}$, respectively.

Fig. 2 displays the temporal evolution of spanwise vortices represented by $\lambda_{i,z}$ contours in the z -plane at the angled part of the louver at $z = -1.46$. For presentation purpose, the vortices are labeled by letters, and a “+” sign implies vortices shed from the bottom surface of the leading edge and a “-” sign implies those shed from the top louver surface. The numbers denote the magnitude

² This is calculated a-posteriori by extracting the time mean wall shear stress from the calculation. For reference, a fully turbulent channel flow calculation is adequately resolved by the current procedure with five grid points within 10 wall units normal to the wall, and a resolution of approximately 30 and 10 wall units in the streamwise and spanwise directions, respectively.

³ Tube depth is used in the same context as flow depth. In our calculations, the flow depth is infinity. So a typical value of 15 is used.

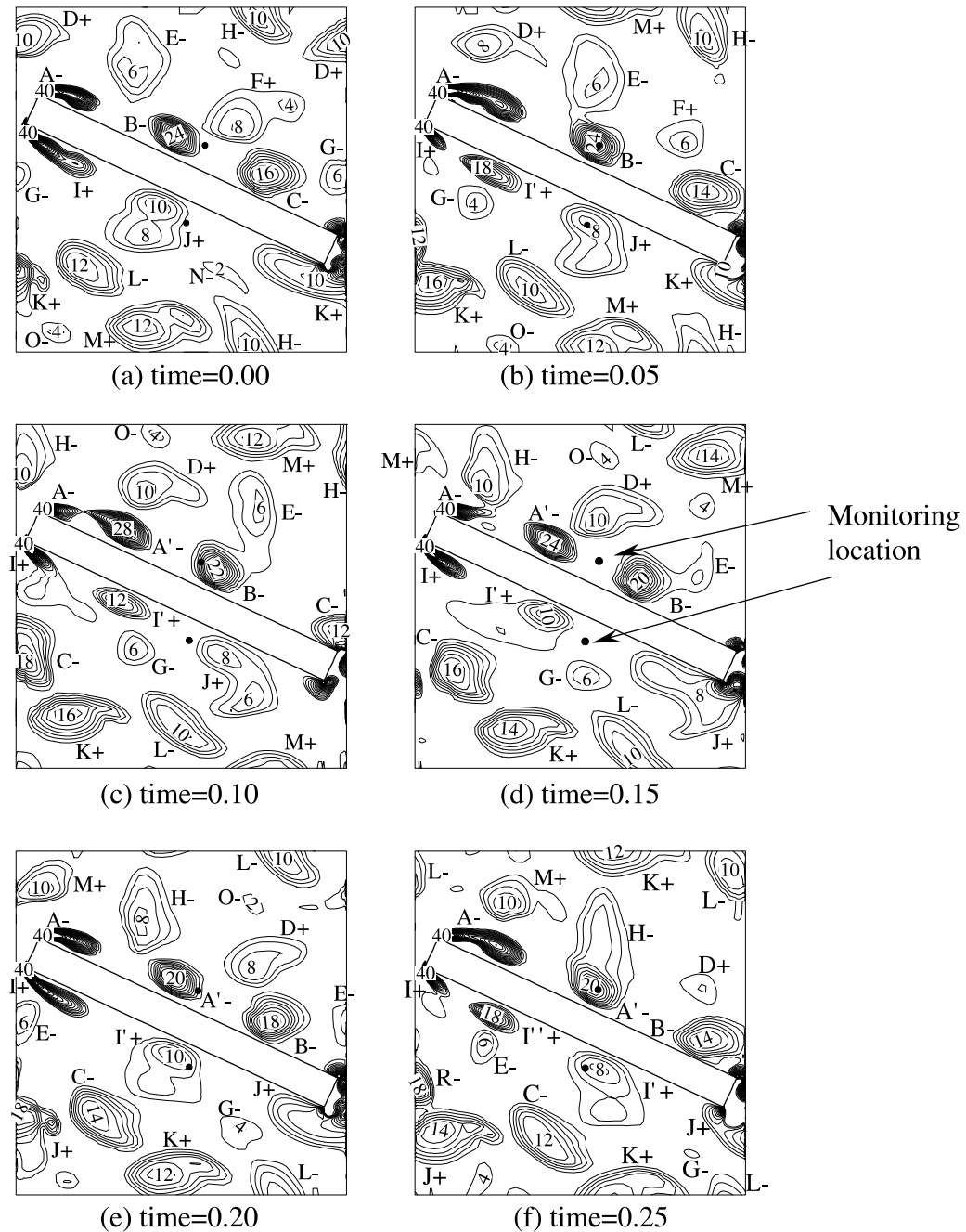


Fig. 2. Temporal evolution of coherent spanwise vortices represented by $\lambda_{i,z}$ contours in the z -plane at $z = -1.46$. Contour levels are in steps of 2 ranging from 0 to 40. Vortices shed from the leading edge, combine with wake vortices and also interact with upstream shed vortices.

of $\lambda_{i,z}$ at the vortex center. At time $t = 0.00$, Fig. 2(a), vortex shedding from both top and bottom surface at the leading edge is clearly evident, in spite of the flow not being completely aligned with the louver. Near the leading edge, vortex A^- and I^+ have the same strength

and I^+ is about to shed another vortex. However, comparison of the strength of vortices shed from the top and bottom surface (vortex B^- and J^+ , vortex C^- and K^+) show significant differences. The vortices shed from the top surface are a factor of 2–3 stronger than those

shed from the bottom edge.⁴ We also see strong interactions between leading and trailing edge vortices. The trace of vortex K^+ in Fig. 2(a–c), J^+ in Fig. 2(d–f), and C^- in Fig. 2(b–e), suggests that vortices shed from the leading edge shear layer, merge with vortices at the trailing edge and pick up strength before convecting into the wake.

Because of the periodicity, vortices leaving the domain, re-enter the domain again (see vortex D^+ , H^- , G^- and K^+). The corresponding spatial interpretation of vortex trajectories shed from a louver is shown in Fig. 3(a). In the snapshot at $t = 0.0$, the immediate wake of the louver is represented by the alternating vortices (K^+ , L^- , M^+ , H^-), which convect further downstream to become (D^+ , E^- , F^+ , G^-). The vortices have a spatial life span of approximately 3–4 louver pitches from the time they are generated at the leading edge.

Vortex–vortex interactions are also observed on the top surface of the louver. At time $t = 0.05$, Fig. 2(b), vortex I'^+ is shed from the shear layer on the bottom surface. Vortex B^- begins to interact with vortex E^- (from the wake of a previous louver) as both move downstream. As they approach the trailing edge, at $t = 0.20$ in Fig. 2(e) they separate again. Similar interactions can also be observed in Fig. 2(f) between A'^- and H^- . We also take note of the fact that a vortex is always shed from a leading edge shear layer in the presence of a vortex of opposite sign from the wake of a previous louver. For instance, vortex A'^- is shed in the presence of D^+ , whereas I'^+ is shed in the presence of G^- .

The vorticity dynamics observed in Fig. 2 is present throughout the angled portion of the louver, which is dominated by the periodic shedding of spanwise vorticity. Fig. 3(b) plots contours of $\lambda_{i,z}$ in the z -plane at $z = -0.122$, just before the louver starts its transition, at one instant in time, $t = 0.00$. The vortices are much more diffuse and weaker in this region. However, in spite of this there is a good correlation with Fig. 2(a), and the flow is still preferentially two-dimensional with weak three-dimensional effects.

Fig. 3(c–d) shows the time history and corresponding frequency spectrum, respectively, of the temperature signal at the angled louver close to the plane of symmetry. The monitoring location is above the top louver surface and at the middle of the louver. The time signals exhibit a nearly periodic pattern, which is consistent with the periodic vortex shedding from the leading edge on the louver top surface observed from the flow animations. The frequency spectrum shows a clear peak at $f \approx 5.2$, which corresponds to the frequency of vortex shedding observed in Fig. 2. Based on louver pitch and

the bulk velocity, the characteristic non-dimensional frequency is 1.87. This value compares well with the value of 2 obtained in previous two-dimensional calculations [6] of developing flow and heat transfer in multilouvered fins.

There is considerable evidence in Fig. 2 that vortex shedding from a louver does not proceed in isolation but is influenced by other louvers as well, until a characteristic “louver bank” frequency is established. This agrees with the experiments of Mochizuki and Yagi [21] and also our two-dimensional numerical studies [6]. Mochizuki and Yagi [21] in their experiments with staggered fin arrangements, found that multiple frequencies were observed for arrays which were less than eight columns deep, however, once the depth of the array increased beyond this point, single characteristic frequencies were found, thus indicating that vortex shedding in large arrays was influenced by factors other than individual plates. Tafti and Zhang [6], in two-dimensional developing flow in multilouvers also reached similar conclusions. They found that the characteristic frequencies did not scale with louver thickness, as it would in the case of isolated plates, but scaled with a length scale associated with the fin pitch, and postulated from this that the interaction of convecting vortices played a major role in fixing the characteristic frequency.

The flow takes on added complexity in the transition region. It is strongly three-dimensional and the flow dynamics are quite different. To illustrate this, Fig. 4(a) plots the distribution of volume averaged $\lambda_{i,x,y,z}$ as a function of fin height at an arbitrary instant in time. Only the volumes with non-zero eigenvalues are included in the volume averaging. On the angled louver, λ_i essentially maintains a constant value, with a dominant contribution from spanwise vorticity. However, in the transition region, λ_i increases, with increasing contributions from streamwise and cross-stream vorticity, with a drop in contributions from spanwise vortices. λ_i reaches a maximum in the center of the transition region and then decreases as the louver approaches the flat landing and the tube surface.

Fig. 4(b) plots the surface contours of $\lambda_i = 30$ at the bottom of the louver in the transition region. This includes all components of coherent vorticity. An agglomeration of coherent vorticity is found at the leading edge of the louver at all time instances. This is mostly spanwise vorticity which is formed by the interaction of the flow with the leading edge. The elongated zone of vorticity near the junction with the flat landing mostly consists of contributions from streamwise and cross-stream vorticity and is the coherent core of a “vortex jet” which forms in this region. The decreasing flow area between two adjacent louvers, adds considerable translational energy to the flow between louvers. Part of the flow accelerates over the top surface, while the remaining part is drawn underneath the louver. The sweep

⁴ The vortices shed from the leading edge of the bottom surface are weak and are difficult to sense without isolating them from the background vorticity.

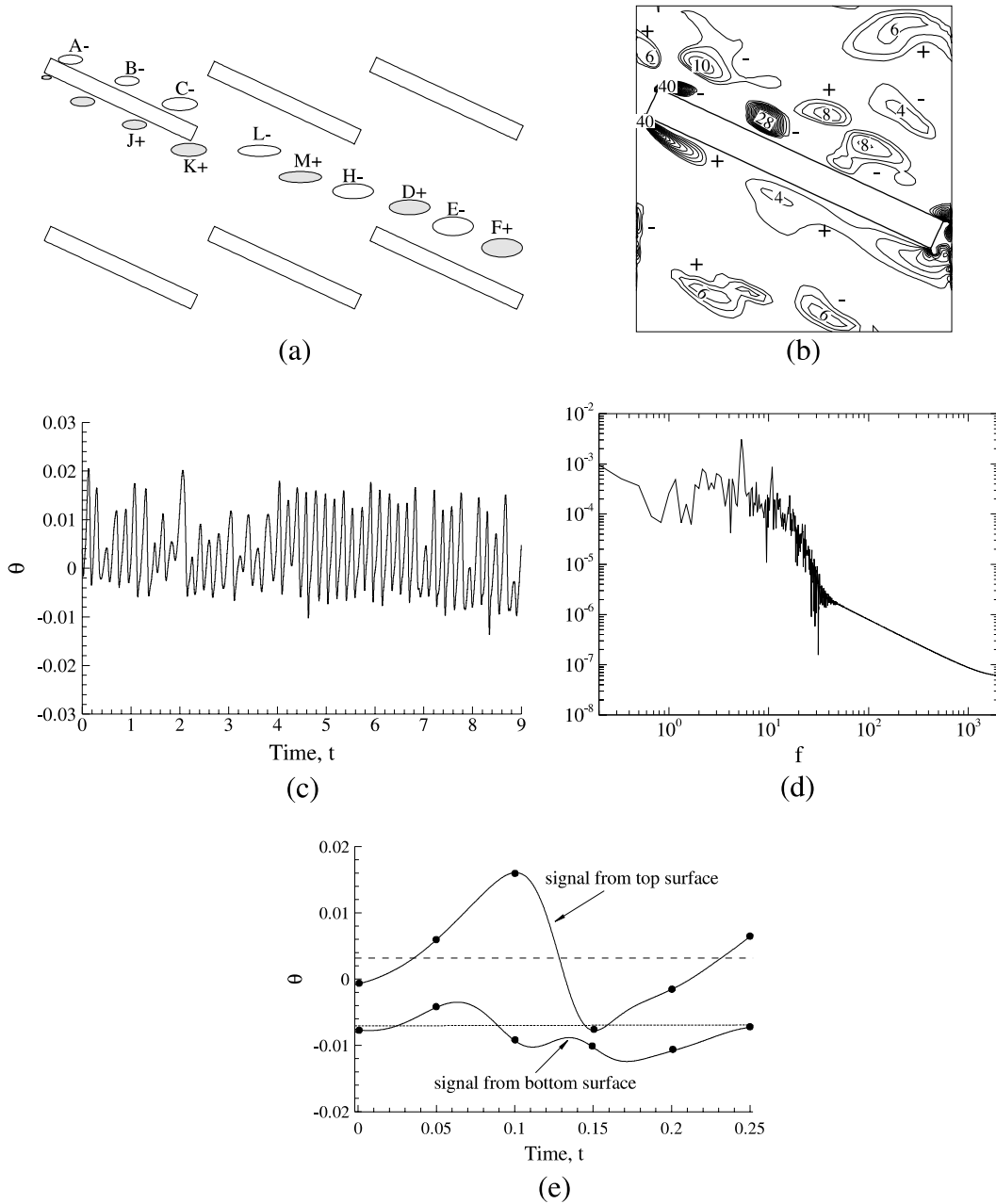


Fig. 3. (a) Trajectory of vortices shed from a single louver as derived from Fig. 2; (b) contours of $\lambda_{i,z}$ at time $t = 0.00$ in the z -plane at $z = -0.122$, just before the start of the transition region. Vortices are diffuse and weaker than at $z = -1.46$; (c) temperature signal and (d) frequency spectrum at plane $z = -1.46$ in the angled louver portion. The monitoring location is near the middle of louver and is 0.065 in normal distance from the louver top surface; (e) temporal evolution of temperature on the top and bottom surface of the louver corresponding to the vortex shedding cycle shown in Fig. 2.

angle of the leading edge in turn adds rotational energy to the flow which is drawn underneath the louver. This results in a region of concentrated streamwise vorticity, which forms the core of the vortex jet. In general the vortex jet follows a trajectory away from the tube sur-

face and towards the angled louver. It also moves away from the louver surface. We also observe that the core, which is made up of the elongated zone of vorticity, periodically forms and detaches from the leading edge on a time scale of about $t = 0.2$.

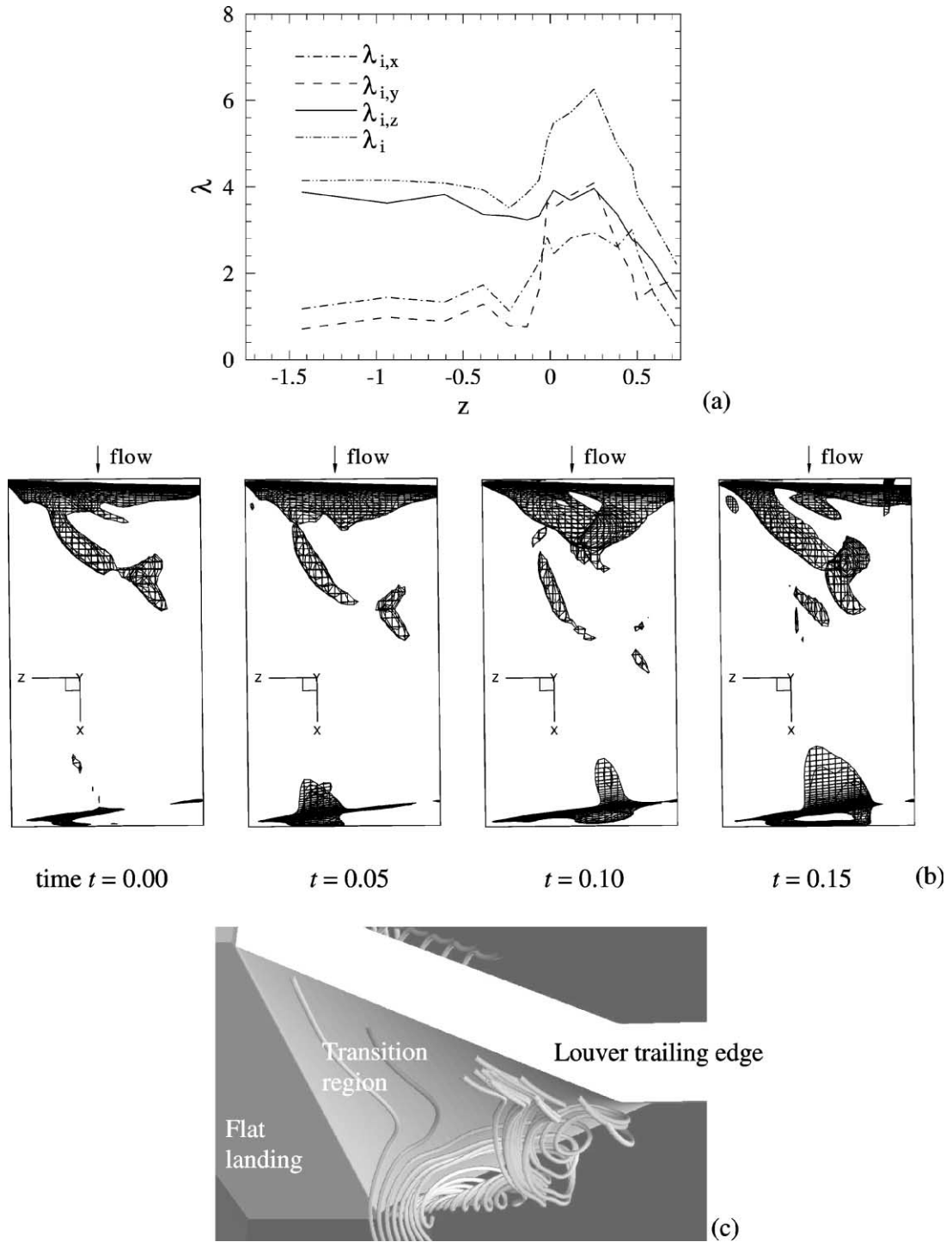


Fig. 4. (a) Volume-averaged vortical strength distribution along the fin height at an arbitrary instant; (b) surface contours of $\lambda_i = 30$ at the bottom of the louver in the transition region. There is periodic formation and detachment of vorticity from the leading edge region; (c) instantaneous streamtubes injected near the leading edge of the louver near the junction with the flat landing, seen from louver bottom.

Fig. 4(c) plots a snapshot of instantaneous stream tubes injected in the leading edge region of the louver. A region of intense rotation can be identified near the leading edge. In spite of the small spatial extent of the core, the intense rotational energy entrains fluid from the surroundings it grows and quickly loses its coherency within half a louver length.

Fig. 5(a–d) plots the time signals of temperature, and the respective spectra at two locations in the transition region. One location is in the middle of the transition region at $z = 0.243$ and the other nearer the flat landing at $z = 0.424$, both on the top surface of the louver. The signals are more chaotic and exhibit a higher energy content than their counterparts in the vicinity of the angled louver. There is no clear indication of a characteristic frequency as in Fig. 3. However, at both locations there is considerable low frequency energy in the signal. The strong low frequency content is quite pronounced in Fig. 5(c–d) at the location near the flat

landing, at a frequency of approximately 0.3. This is also present in Fig. 5(a–b), but is not as well defined. Similar observations are made at the bottom of the louver, for both temperature and velocity fluctuations. The discussion on the cause of the low frequency oscillation and its dynamics and effect on heat transfer is deferred to the next section.

In summary, the periodic shedding of spanwise vortices dominates the flow field on the angled part of the louver. Because the flow is nearly aligned with the louver direction, vortices are shed from both the top and bottom leading edges, however, the vortices shed from the top are 2–3 times stronger. There is considerable interaction between vorticity shed from the leading and trailing edge of louvers, and also between louvers. The dynamics of vortex shedding in this region is nominally two-dimensional. In the transition region, the flow is strongly three-dimensional. It is dominated by an unsteady vortex jet, which flows underneath the louver,

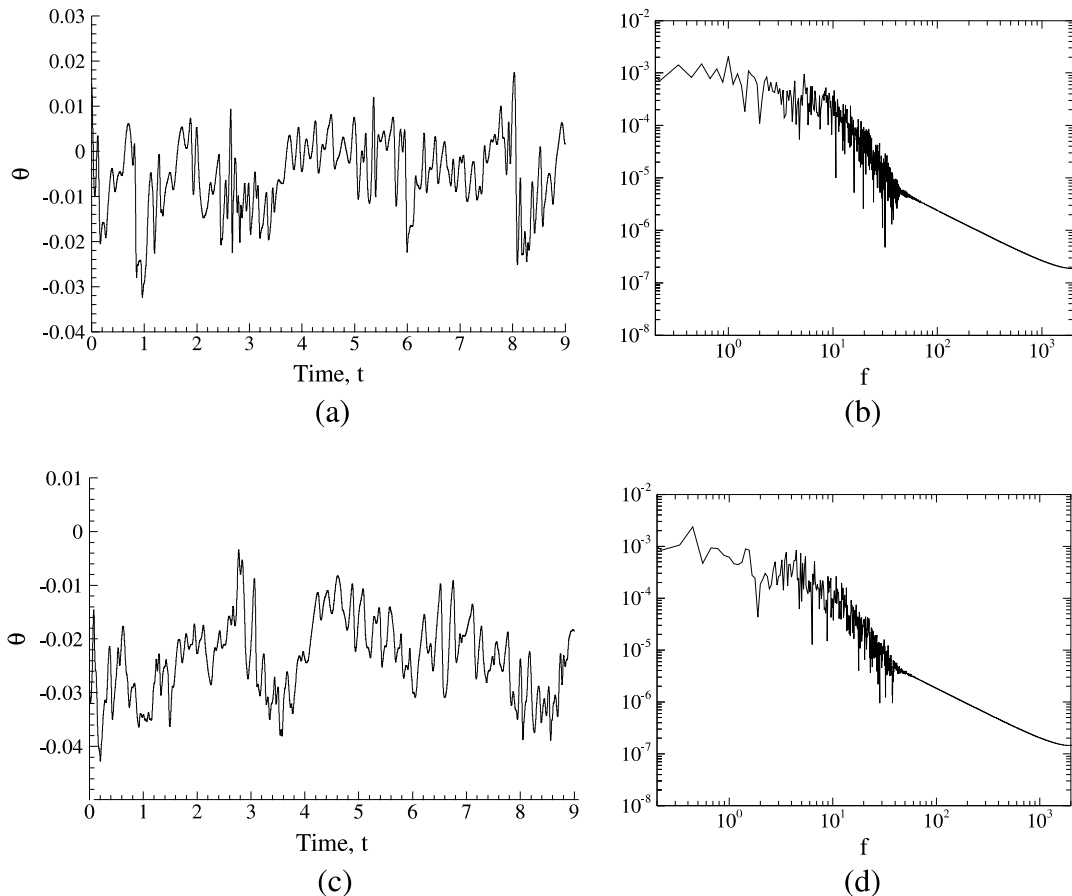


Fig. 5. Signal analysis at plane $z = 0.243$ near the middle of the transition region: (a) temperature signal (b) temperature frequency spectrum. The monitoring location is near the middle of louver and is 0.060 in normal distance from the louver top surface; similar signal analysis at plane $z = 0.424$ near the flat landing: (c) temperature signal (d) temperature frequency spectrum. The monitoring location is near the middle of louver and is 0.052 in normal distance from the louver top surface.

and strong flow acceleration. The region is characterized by nearly equal contributions from all three components of coherent vorticity, with a net increase in overall magnitude. Time signals and spectral plots indicate a quasi-periodic low frequency oscillation in this region.

4.2. Unsteady heat transfer characteristics

Here we evaluate the effect of the unsteady flow field on the instantaneous heat transfer on the louver surface. On the angled louver, the heat transfer is dominated by the impinging flow on the bottom of the louver surface and the spanwise vortices on the top surface. It has been established in previous studies [10] that spanwise vortices act as large-scale mixers. The augmentation in heat transfer depends on the strength of the vortex and its location with respect to the surface [10]. Vortices embedded at the edge of the boundary layer, through their rotational energy bring in free-stream fluid in the vicinity of the heat transfer surface. The induced fluid mass then picks up heat from the surface and is ejected back into the free-stream. Fig. 3(e) plots the temporal evolution of temperature on the top and bottom surface of the louver corresponding to the vortex shedding cycle shown in Fig. 2. The measurement locations are located at $z = -1.46$ near the middle of the louver and are shown in Fig. 2. The temperature variation with time corresponds to the passing of vortex B^- and then A'^- on the top surface and vortex J^+ and I^+ on the bottom surface. On the downstream side of the vortex, free-stream fluid is induced towards the louver, resulting in the low temperature valley at $t = 0.15$ corresponding to vortex A'^- . As the vortex convects downstream of the measurement location a peak in temperature results as the heat carrying fluid is ejected out back into the free-stream. This occurs at $t = 0.10$ after the passage of vortex B^- . The passage of vortices on the bottom surface do not have a large effect on heat transfer.

Fig. 6 plots the temporal evolution of local surface-averaged Nusselt numbers from $z = 0.25$ to 0.5 in the transition region near the flat landing. Both, the top and bottom surface of the louver show large quasi-periodic variations in Nusselt number at intervals of approximately 2–3 non-dimensional time units. The Nusselt number on the top surface is characterized by short bursts of intense activity in the region near the flat landing, with relatively long periods of calm. Activity is more frequent and less intense on the louver bottom surface. The events which lead to the fluctuations in Nusselt number occur around the same time on both the top and bottom surface indicating that the two are correlated.

To understand what causes the large increase in the local Nusselt number on the top surface, Fig. 7(a–d) plots the instantaneous velocity vectors and temperature contours on the top surface in a z -plane ($z = 0.424$) near

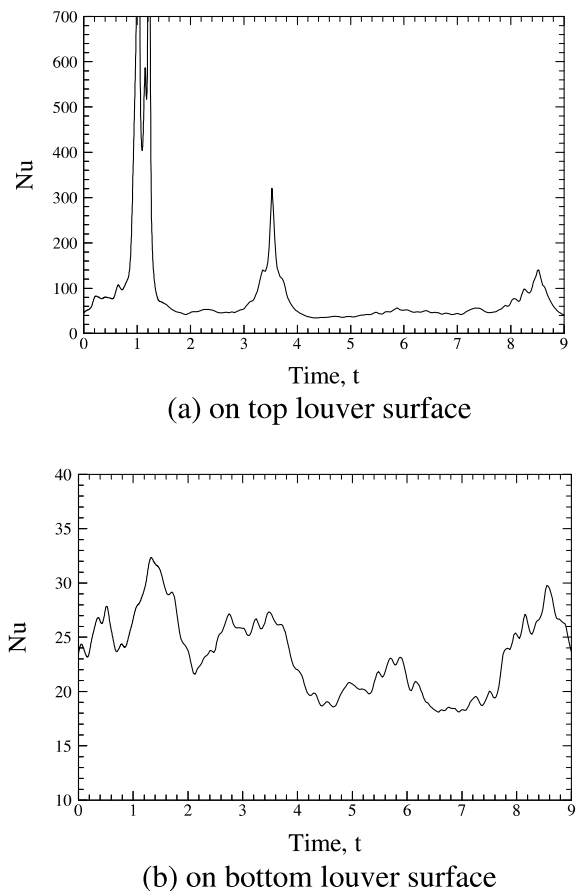


Fig. 6. Temporal evolution of surface-averaged Nusselt numbers from $z = 0.25$ to 0.5 in the transition region near the flat landing. The low frequency events on the top and bottom surface are correlated.

the flat landing. The vectors are plotted at three locations along the length of the louver. At $t = 3.5$, when the Nusselt number on the top surface is high, the flow velocity in the vicinity of the louver is very high, which significantly reduces the thickness of the thermal boundary layer and leads to very high heat transfer. The resulting effect on the temperature of the louver surface is shown in Fig. 7(b). A low temperature zone exists (high heat transfer) in the region near the flat landing, which extends throughout the length of the louver. Whereas at $t = 4.5$, the flow velocity is not as energetic and subsequently its effect on louver heat transfer is not quite that strong. We note that even in its non-energetic state, the high velocities near the top surface provide enhanced heat transfer compared to the angled portion of the louver.

The dynamics of Nusselt number fluctuations on the bottom surface is related to the dynamics of the vortex jet and its effect on the flow. Fig. 8(a–f) plots instantaneous

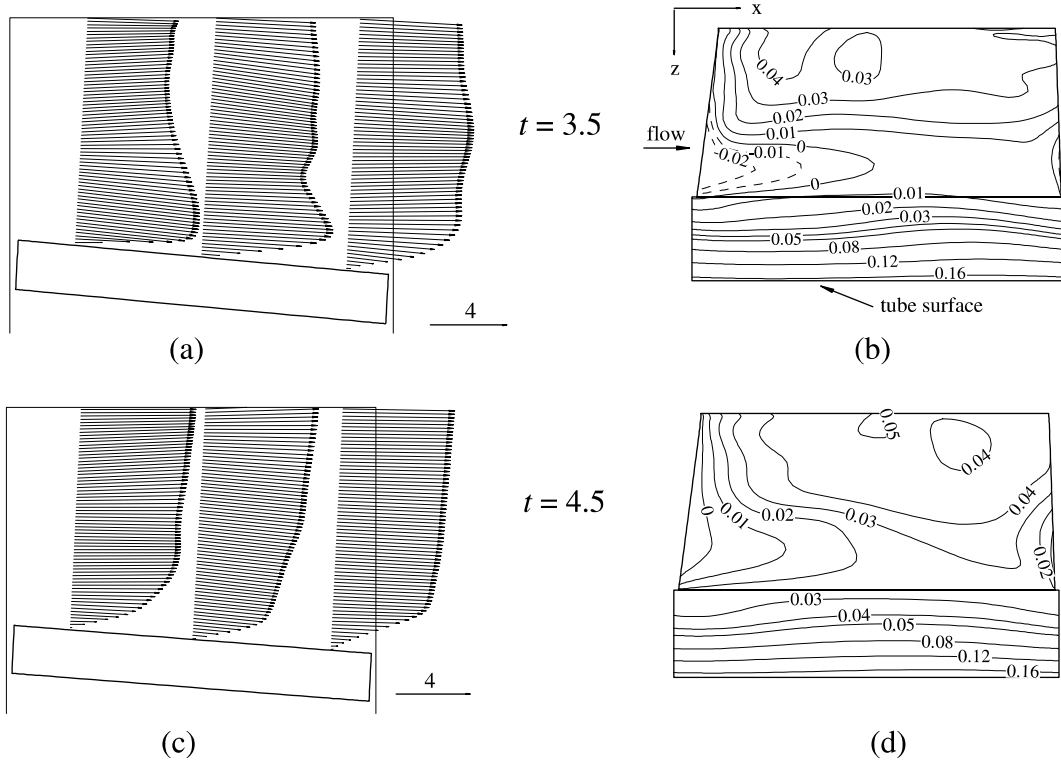


Fig. 7. (a) Instantaneous velocity vectors and (b) temperature contours on the top surface in a z -plane at $z = 0.424$ in the transition region near the flat landing at time $t = 3.5$; (c) instantaneous velocity vectors and (d) temperature contours at the same location at time $t = 4.5$. The accelerating flow on the top surface increases heat transfer. Arrow shows scaling of vectors.

surface contours of $\lambda_i = 30$ in the transition region at $t = 1.5$ and 4.5 , corresponding to a peak and valley, respectively, in Fig. 6. At $t = 4.5$, the vortex jet is dominant in the leading edge region and its proximity to the surface induces a recirculation zone underneath it in the leading edge region. Hence during this state the jet has a detrimental effect on heat transfer which can be surmised from Fig. 8(f). A region of high surface temperature and low heat transfer correlates roughly with the location of the vortex jet. On the other hand at $t = 1.5$, the vortex jet has detached from the leading edge region and the core that remains attached has a different spatial location and orientation. Again, we find that the instantaneous temperature contours on the surface correlate with the location of the jet. However, unlike at $t = 4.5$, the temperatures are much lower, not only in the vicinity and underneath the jet but also in the vicinity of the trailing edge of the louver. The substantially lower temperatures near the trailing edge is due to increased flow velocity, which is caused by the formative vortex jet at the leading edge of the louver downstream.

We postulate a scenario in which the dynamics of the vortex jet underneath the louver affects the movement of fluid on the top surface of the louver or vice versa. The location, state, and strength of the vortex jet affects the

trajectory of fluid on the top surface. From the evidence we have seen, it seems that a strong attached vortex jet at the bottom pushes the high velocity fluid on the top surface away from the louver surface and limits the heat transfer augmentation. When the vortex jet destabilizes, detaches and starts forming again, high velocity fluid on the top surface is drawn to the vicinity of the louver surface which results in high heat transfer. At the same time, the detached jet and its subsequent formation also increases heat transfer on the bottom surface. In addition to this occurring on a long time scale ($t = 2-3$), the jet also destabilizes and forms on a much shorter time scale of $t = 0.2-0.3$, as seen in Fig. 4. Correspondingly, the extent of the high velocity region in the vicinity of the top louver surface also oscillates. This can be clearly discerned from flow animations. However, the fast time scale variations are not as strong and sustained as the long time scale variations.

4.3. Mean flow and heat transfer

Fig. 9(a-d) shows the time mean velocity vectors at four z -planes. At the angled louver part (Fig. 9(a)), the vectors are quite parallel to the louver surface, indicating the flow is essentially louver-directed at this Reynolds

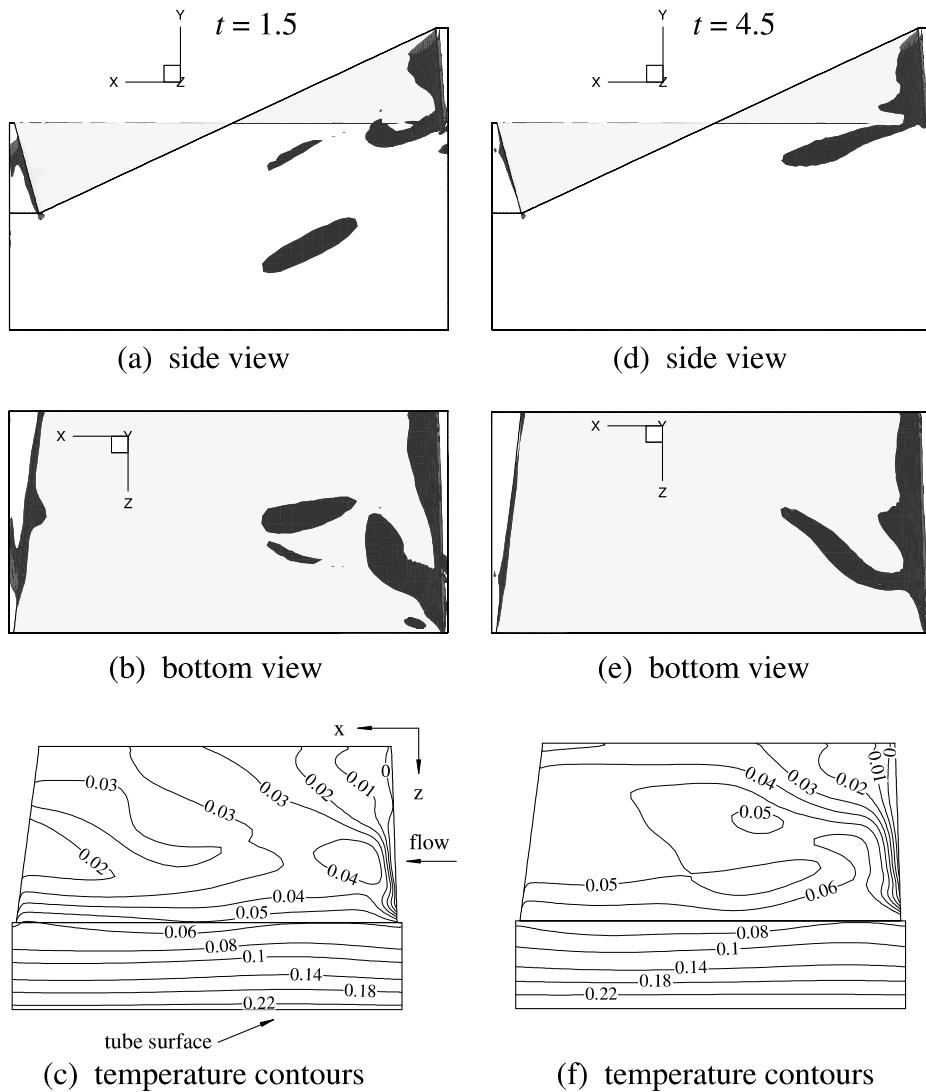


Fig. 8. (a) Side view and (b) bottom view of instantaneous surface contours of $\lambda_i = 30$ in the transition region, and (c) the temperature contours on the louver bottom surface at time $t = 1.5$; (d) side view and (e) bottom view of the instantaneous surface contour of $\lambda_i = 30$ in the transition region, and (f) the temperature contours on the louver bottom surface at time $t = 4.5$. The heat transfer on the bottom surface is closely related to the dynamics of the vortex jet.

number and louver angle. Near the leading edge on the louver top surface, a mean recirculation zone can be identified which is a result of the separated shear layer at the leading edge. Away from the surface, the flow recovers quickly and a velocity overshoot represents the separated shear layer. At the middle of the louver, flow reattaches to the louver surface and a boundary layer starts to develop. The boundary layer grows as the flow moves downstream toward the trailing edge. At this location, the vectors far away from the louver surface show a downward motion as the flow approaches the leading edge of the downstream louver. On the louver bottom, the flow remains attached and the boundary

layer grows as the flow proceeds downstream. The wake of the upstream louver is visible at the first two locations and recovers gradually as the flow moves further downstream.

In the transition region, the flow field is quite different (Fig. 9(b)). This z -plane is at the middle of the transition zone and the louver angle has decreased from 25° in the angled louver part to 10.4° . Although not represented in Fig. 9(b), the flow is three-dimensional with substantial momentum transport occurring along the fin height or spanwise direction. On the top surface, near the leading edge and at the louver middle, the velocity distribution appears to be nearly uniform with

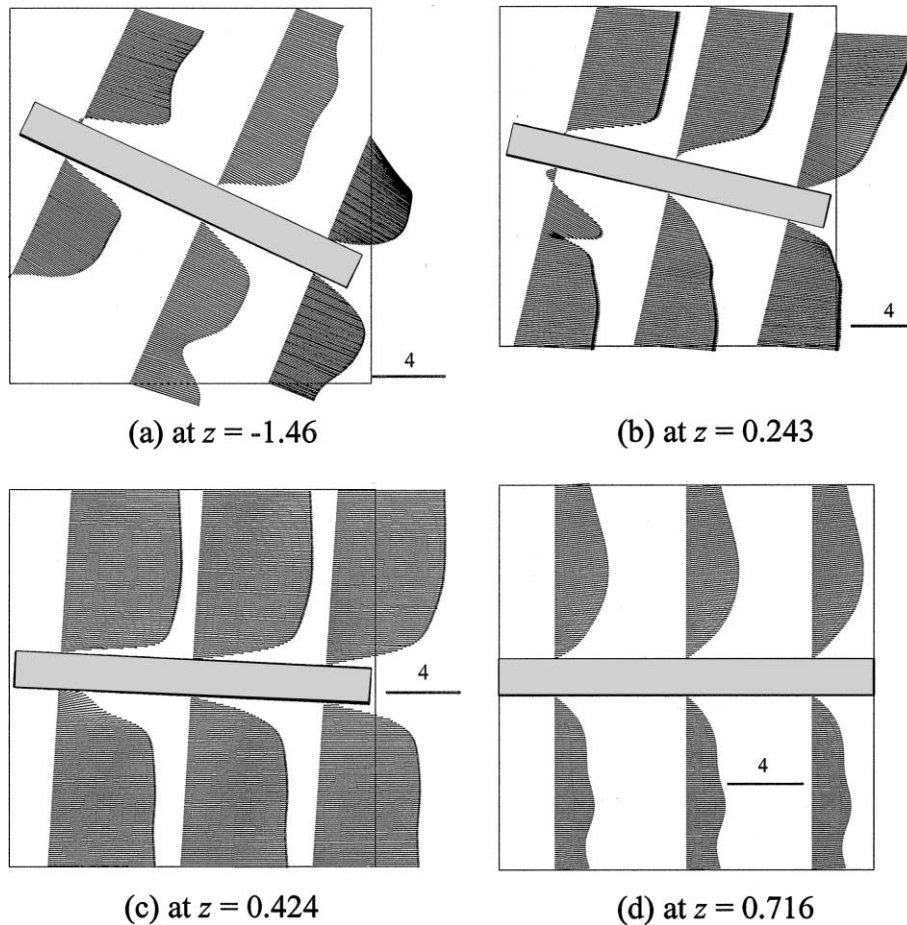


Fig. 9. Time mean velocity vectors at four z -planes: (a) on the angled louver; (b) at the middle of the transition region; (c) near the flat landing; (d) on the flat landing. The acceleration in the transition region is clear. Arrow shows scaling of vectors.

large defects in the vicinity of the louver. At the last station, the velocity profile has recovered, most likely from spanwise and cross-stream momentum transfer, as the flow near the louver is drawn down into its wake. On the other hand, flow away from the louver surface flows over the leading edge of the downstream louver. The first profile on the bottom of the louver captures the initial core of the vortex jet before it moves out of the plane. As explained in the previous section, the jet forms as a consequence of the translational and rotational energy imparted to the fluid in this region. The strong shear layer of the jet produces a recirculation zone underneath it on the louver surface.

Fig. 9(c) shows similar profiles at a location near the flat landing at $z = 0.424$. Large fluid velocities are evident on the top surface of the louver particular in the region immediately following the leading edge. This plane is in the region where the shear stress reaches a maximum and the velocity profiles are closest to that in a turbulent flow over a flat plate. In this region, the flow

area between louvers narrows considerably. Hence flow from the top surface of the louver is not drawn underneath in its wake. Consequently, it impinges on the leading edge of the following louver and accelerates over the top surface. The flow at the bottom of the louver also moves in the streamwise direction at the trailing edge and impinges on the bottom surface of the downstream louver as seen in Fig. 9(c).

On the flat landing (Fig. 9(d)), as we approach the tube surface at $z = 0.716$, the velocity decreases considerably as it is engulfed in the boundary layer on the tube surface. However, we find that the velocity in the vicinity of the top surface is higher than at the louver bottom. This is due to the residual effect of the strong flow velocities in its vicinity. Although, the profiles imply that the flow is laminar and steady, flow animations show that the boundary layer on the tube surface, although laminar, is not steady and undulates on a long spatial and temporal wavelength in response to the flow dynamics adjacent to it in the transition region.

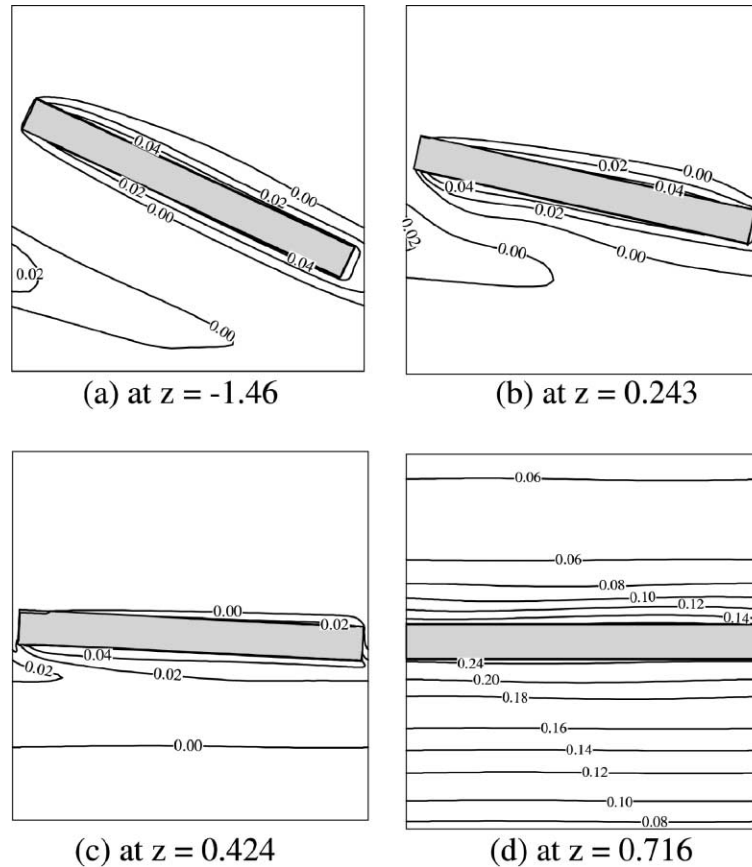


Fig. 10. Mean thermal fields in four z -planes: (a) on the angled lower portion; (b) at the middle of the transition region; (c) near the flat landing; (d) on the flat landing.

Fig. 10(a–d) shows thermal fields at the angled louver portion, transition zone, and flat landing. One of the consequences of the louver flattening out is that the thermal wake of the louver starts interfering with the bottom surface of the louver immediately downstream of it. Hence in this region, the combination of the thermal wake effect and the recirculation zone induced by the vortex jet reduces the heat transfer coefficient on the lower surface of the louver. On the other hand, the high velocity on the top surface and its close proximity to the louver surface increases the heat transfer coefficient. This can be surmised by the relatively thin thermal boundary layer on the top surface in the transition region. In the angled part of the louver, the thermal boundary layer on the top surface is thicker than that on the bottom surface of the louver. Generally, the effect of the large-scale vortices is to shorten the mean recirculation region and enhance heat transfer downstream of it. On the bottom surface, because the oncoming flow impinges near the leading edge, the thermal boundary layer is thinnest in this region and increases downstream. At the flat landing, temperatures are much higher since

the flow is engulfed in the louver as well as the tube thermal boundary layer. However, we find that the thermal boundary layer on the top surface is much thinner than that on the lower surface.

Fig. 11(a–b) plots the time mean thermal field on the top and bottom surface of the louver. A high surface temperature implies low heat transfer. On the top surface of the angled louver, the temperatures are lowest in the leading edge region, and increase as we travel downstream up to the mean reattachment line which occurs at about $x = 0$. Downstream of the mean reattachment line, the temperatures decrease due to the enhancement provided by spanwise vortices. On the lower surface, the temperatures are lowest in the vicinity of the leading edge and increase downstream. In the transition region, the mean temperatures follow the major unsteady flow features, outlined in the previous section. The high heat transfer region on the top surface near the flat landing is caused by the flow acceleration in the vicinity of the louver surface. On the other hand, a low heat transfer region is formed on the bottom surface due to the presence of the vortex jet. The low heat transfer

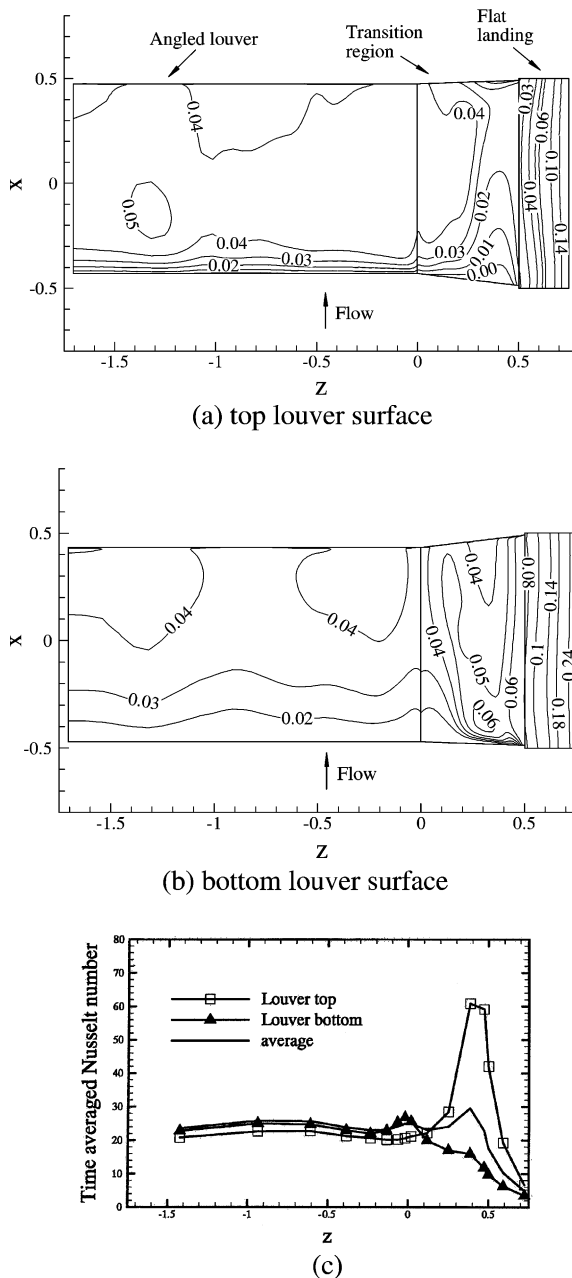


Fig. 11. Mean thermal field distribution: (a) on the top and (b) bottom surface of louver; (c) time-averaged mean Nusselt number distribution along the fin height averaged over time 4.5–9.

region near the leading edge is a result of a mean recirculation zone formed underneath the jet. On the flat landing, near the tube surface, the mean heat transfer is much higher on the top surface than the bottom surface.

Fig. 11(c) plots the variation of local mean Nusselt number across the fin height. The results are averaged

from $t = 4.5$ to 9. The Nusselt number is fairly constant on the angled louver up to the beginning of transition. As expected, in this region the Nusselt number is higher on the bottom surface, because of flow impingement and the absence of a mean recirculation region. In the transition region, the Nusselt number drops gradually on the lower surface but increases sharply on the top surface to more than twice its value. On the flat landing the Nusselt number drops to 4.1 and 7.3, respectively, on the bottom and top surface of the louver near the tube.

The mean Nusselt number integrated over the part of the louver simulated in the current study was found to be 20. On the tube surface the corresponding mean Nusselt number was calculated to be 7.2. Although, the transition region does provide some augmentation of heat transfer on the louver surface, its overall impact on louver heat transfer is limited because of its small spatial extent. However, the transition geometry does have a positive impact on tube heat transfer. In a separate calculation, which extended the angled louver to the tube surface, and which excluded the transition and flat landing, found that the Nusselt number on the tube surface was lower by a factor of 1.5.

5. Conclusions

The flow and heat transfer in a three-dimensional geometry of a multilouvered fin is studied. The geometry includes the angled part of the louver and its transition to the flat landing along the fin height. Although the results shown here correspond to one Reynolds number for a given geometry, we believe that qualitatively the flow and heat transfer will show similar characteristics for other geometries as well.

The flow on the angled louver is characterized by spanwise vortex structures which are shed from the separated shear layers on the top and bottom surface of the louver. The flow is nominally two-dimensional with weak three-dimensionality. There is considerable interaction between vorticity shed from the leading edge of the louver and that formed in the wake of the louver. There is also strong evidence of interactions with vortices shed from upstream louvers. Vortices shed from the leading edge have a spatial life span between 3 and 4 louver lengths before they dissipate.

In the transition region, the flow is strongly three-dimensional and unsteady. It is characterized by strong streamwise flow velocities in the vicinity of the top louver surface near the junction with the flat landing and the formation of a vortex jet underneath the louver. There is evidence that the temporal evolution of the two are correlated. Both the high velocity region and the vortex jet oscillate on a short as well as a long time scale. However, the long time scale or low frequency oscillations are much stronger and persist for a longer time. It

is suspected that both time scales are related to the formation and detachment of the vortex jet from the leading edge region. The flow characteristics isolated in the transition region will play a potentially important role in condensate carryover because of the high induced shear stresses.

In spite of the high heat transfer in this region, the overall effect on louver mean heat transfer is small because of the small spatial extent of the transition region. But, the strong acceleration near the junction with the flat landing does improve tube surface heat transfer by over 50% when compared to a geometry in which the angled louver extends all the way to the tube surface.

Acknowledgements

Dr. J. Cui was partially supported by the Air Conditioning and Refrigeration Center, Department of Mechanical and Industrial Engineering, University of Illinois at Urbana-Champaign. Supercomputing time was granted by the NSF PACI program through the National Resource Allocation Committee (NRAC). The authors would also like to acknowledge the contributions made by Randy Heiland, NCSA, in flow visualization and Dr. Weicheng Huang, NCSA in grid generation at the University of Illinois at Urbana-Champaign.

References

- [1] D.K. Tafti, L. Zhang, G. Wang, Time-dependent calculation procedure for fully developed and developing flow and heat transfer in louvered fin geometries, *Numer. Heat Transfer, Part A* 35 (1999) 225–249.
- [2] D.K. Tafti, X. Zhang, W. Huang, G. Wang, Large-eddy simulations of flow and heat transfer in complex three-dimensional multilouvered fins, Invited paper, paper no. FEDSM2000-11325, *CFD Applications in Automotive Flows*, 2000 ASME Fluids Engineering Division Summer Meeting, June 11–15, Boston, Massachusetts, 2000.
- [3] C.J. Davenport, Heat transfer and flow friction characteristics of louvered heat exchanger surfaces, in: J. Taborek, G.F. Hewitt, N. Afgan (Eds.), *Heat Exchangers: Theory and Practice*, Hemisphere, Washington, DC, 1983, pp. 397–412.
- [4] R.L. Webb, P. Trauger, Flow structure in the louvered fin heat exchanger geometry, *Exp. Therm. Fluid Sci.* 4 (1991) 205–217.
- [5] X. Zhang, D.K. Tafti, Classification and effects of thermal wakes on heat transfer in multilouvered fins, *Int. J. Heat Mass Transfer* 44 (2001) 2461–2473.
- [6] D.K. Tafti, X. Zhang, Geometry effects on flow transition in multilouvered fins—onset, propagation, and characteristic frequencies, *Int. J. Heat Mass Transfer* 44 (2001) 4195–4210.
- [7] D.K. Tafti, G. Wang, W. Lin, Flow transition in a multilouvered fin array, *Int. J. Heat Mass Transfer* 43 (2000) 901–919.
- [8] L.W. Zhang, D.K. Tafti, F.M. Najjar, S. Balachandar, Computations of flow and heat transfer in parallel-plate fin heat exchangers on the CM-5: effects of flow unsteadiness and three-dimensionality, *Int. J. Heat Mass Transfer* 40 (1997) 1325–1341.
- [9] L.W. Zhang, S. Balachandar, D.K. Tafti, F.M. Najjar, Heat transfer enhancement mechanisms in inline and staggered parallel-plate fin heat exchangers, *Int. J. Heat Mass Transfer* 40 (1997) 2307–2325.
- [10] L.W. Zhang, S. Balachandar, D.K. Tafti, Effect of intrinsic three dimensionality on heat transfer and friction loss in a periodic array of parallel plates, *Numer. Heat Transfer Part A* 31 (1997) 327–353.
- [11] D. Halt, personal communication, Visteon Automotive Systems, 1999.
- [12] W.J. McLaughlin, R.L. Webb, Condensate drainage and retention in louver fin automotive evaporators, SAE Technical Paper 2000-01-0575, 2000.
- [13] E.M. Sparrow, A. Hajiloo, Measurements of heat transfer and pressure drop for an array of staggered plates aligned parallel to an air flow, *J. Heat Transfer* 102 (1980) 426–432.
- [14] F.N. Beauvais, An aerodynamic look at automobile radiators, SAE Paper no. 65070, 1965.
- [15] L.W. Zhang, personal communication, Modine Manufacturing Company, 2000.
- [16] S.V. Patankar, C.H. Liu, E.M. Sparrow, Fully developed flow and heat transfer in ducts having streamwise-periodic variations of cross-sectional area, *J. Heat Transfer* 99 (1977) 180–186.
- [17] J. Kim, P. Moin, Application of a fractional step method to incompressible Navier–Stokes, *J. Comput. Phys.* 59 (1985) 308–323.
- [18] Y.-J. Chang, C.-C. Wang, A generalized heat transfer correlation for louvered fin geometry, *Int. J. Heat Mass Transfer* 40 (3) (1997) 533–544.
- [19] M.S. Chong, A.E. Perry, B.J. Cantwell, A general classification of three-dimensional flow fields, *Phys. Fluids A* 2 (5) (1990) 765–777.
- [20] F.M. Najjar, S. Balachandar, Low-frequency unsteadiness in the wake of a normal flat plate, *J. Fluid Mech.* 370 (1998) 101–147.
- [21] S. Mochizuki, Y. Yagi, Characteristics of vortex shedding in plate arrays, in: W. Merzkirch (Ed.), *Flow Visualization II*, Hemisphere, Washington D.C., 1982. pp. 99–103.